DOI:
10.1364/BOE.8.002932

Document Version
Publisher's PDF, also known as Version of record

Research Article | Vol. 8, No. 6 | 1 Jun 2017 | BIOMEDICAL OPTICS EXPRESS 2932
Biomedical Optics EXPRESS

Use of a handheld terahertz pulsed imaging device to differentiate benign and malignant breast tissue

MAARTEN R. GROOTENDORST,[1,2,7] ANTHONY J. FITZGERALD,[3,7] SUSAN G. BROUWER DE KONING,[1,2] AIDA SANTAOLALLA,[1] ALESSIA PORTIERI,[4] MIEKE VAN HEMELRIJCK,[1] MATTHEW R. YOUNG,[2] JULIE OWEN,[5] MASSI CARIATI,[1,2] MICHAEL PEPPER,[4,6] VINCENT P. WALLACE,[3] SARAH E. PINDER,[5] AND ARNIE PURUSHOTHAM[1,2]

[1]*King's College London, Division of Cancer Studies, London, UK*
[2]*Department of Breast Surgery, Guy's and St Thomas' NHS Foundation Trust, London, UK*
[3]*School of Physics, University of Western Australia, Perth, Australia*
[4]*Teraview Ltd., Cambridge, UK*
[5]*King's College London, Division of Cancer Studies, King's Health Partners Cancer Biobank and Breast Pathology Research Group, London, UK;*
[6]*London Centre for Nanotechnology, University College London, UK*
[7]*Contributed equally*
**arniepurushotham@gmail.com*

Abstract: Since nearly 20% of breast-conserving surgeries (BCS) require re-operation, there is a clear need for developing new techniques to more accurately assess tumor resection margins intraoperatively. This study evaluates the diagnostic accuracy of a handheld terahertz pulsed imaging (TPI) system to discriminate benign from malignant breast tissue ex vivo. Forty six freshly excised breast cancer samples were scanned with a TPI handheld probe system, and histology was obtained for comparison. The image pixels on TPI were classified using (1) parameters in combination with support vector machine (SVM) and (2) Gaussian wavelet deconvolution in combination with Bayesian classification. The results were an accuracy, sensitivity, specificity of 75%, 86%, 66% for method 1, and 69%, 87%, 54% for method 2 respectively. This demonstrates the probe can discriminate invasive breast cancer from benign breast tissue with an encouraging degree of accuracy, warranting further study.

OCIS codes: (110.6795) Terahertz imaging; (170.3880) Medical and biological imaging; (170.6935) Tissue characterization.

References and links

1. J. F. I. Soerjomataram, M. Ervik, R. Dikshit, S. Eser, C. Mathers, M. Rebelo, D. M. Parkin, and D. Forman, "GLOBOCAN 2012 v1.0, Cancer Incidence and Mortality Worldwide: IARC CancerBase No. 11" (International Agency for Research on Cancer. World Health Organisation, 2012).
2. R. Jeevan, J. Browne, J. Van der Meulen, J. Pereira, C. Caddy, C. Sheppard, C. McGregor-Johnson, Z. Kramer, and S. Dead, "First Annual Report of the National Mastectomy and Breast Reconstruction Audit 2008" (2008).
3. K. P. McGuire, A. A. Santillan, P. Kaur, T. Meade, J. Parbhoo, M. Mathias, C. Shamehdi, M. Davis, D. Ramos, and C. E. Cox, "Are mastectomies on the rise? A 13-year trend analysis of the selection of mastectomy versus breast conservation therapy in 5865 patients," Ann. Surg. Oncol. **16**(10), 2682–2690 (2009).
4. R. Jeevan, D. A. Cromwell, M. Trivella, G. Lawrence, O. Kearins, J. Pereira, C. Sheppard, C. M. Caddy, and J. H. van der Meulen, "Reoperation rates after breast conserving surgery for breast cancer among women in England: retrospective study of hospital episode statistics," BMJ **345**, e4505 (2012).
5. J. Landercasper, E. Whitacre, A. C. Degnim, and M. Al-Hamadani, "Reasons for re-excision after lumpectomy for breast cancer: insight from the American Society of Breast Surgeons Mastery(SM) database," Ann. Surg. Oncol. **21**(10), 3185–3191 (2014).
6. D. Q. Xue, C. Qian, L. Yang, and X. F. Wang, "Risk factors for surgical site infections after breast surgery: a systematic review and meta-analysis," Eur. J. Surg. Oncol. **38**, 375–381 (2012).

#286058 https://doi.org/10.1364/BOE.8.002932
Journal © 2017 Received 9 Feb 2017; accepted 2 May 2017; published 9 May 2017

Biomedical Optics EXPRESS

7. J. Heil, K. Breitkreuz, M. Golatta, E. Czink, J. Dahlkamp, J. Rom, F. Schuetz, M. Blumenstein, G. Rauch, and C. Sohn, "Do reexcisions impair aesthetic outcome in breast conservation surgery? Exploratory analysis of a prospective cohort study," Ann. Surg. Oncol. **19**(2), 541–547 (2012).
8. D. Arora, S. Hasan, E. Male, R. Abid, C. Ord, E. Dauway, and B. Scott, "Cost analysis of re-excisions for breast conserving surgery in Central Texas," in *ASCO Annual Meeting* (2015)
9. E. R. St John, R. Al-Khudairi, H. Ashrafian, T. Athanasiou, Z. Takats, D. J. Hadjiminas, A. Darzi, and D. R. Leff, "Diagnostic Accuracy of Intraoperative Techniques for Margin Assessment in Breast Cancer Surgery: A Meta-analysis," Ann. Surg. **265**(2), 300–310 (2016).
10. K. Deng, C. Zhu, X. Ma, H. Jia, Z. Wei, Y. Xiao, and J. Xu, "Rapid Discrimination of Malignant Breast Lesions from Normal Tissues Utilizing Raman Spectroscopy System: A Systematic Review and Meta-Analysis of In Vitro Studies," PLoS One **11**(7), e0159860 (2016).
11. J. Q. Brown, T. M. Bydlon, S. A. Kennedy, M. L. Caldwell, J. E. Gallagher, M. Junker, L. G. Wilke, W. T. Barry, J. Geradts, and N. Ramanujam, "Optical spectral surveillance of breast tissue landscapes for detection of residual disease in breast tumor margins," PLoS One **8**(7), e69906 (2013).
12. L. G. Wilke, J. Q. Brown, T. M. Bydlon, S. A. Kennedy, L. M. Richards, M. K. Junker, J. Gallagher, W. T. Barry, J. Geradts, and N. Ramanujam, "Rapid noninvasive optical imaging of tissue composition in breast tumor margins," Am. J. Surg. **198**(4), 566–574 (2009).
13. M. D. Keller, S. K. Majumder, M. C. Kelley, I. M. Meszoely, F. I. Boulos, G. M. Olivares, and A. Mahadevan-Jansen, "Autofluorescence and diffuse reflectance spectroscopy and spectral imaging for breast surgical margin analysis," Lasers Surg. Med. **42**(1), 15–23 (2010).
14. A. M. Laughney, V. Krishnaswamy, E. J. Rizzo, M. C. Schwab, R. J. Barth, Jr., D. J. Cuccia, B. J. Tromberg, K. D. Paulsen, B. W. Pogue, and W. A. Wells, "Spectral discrimination of breast pathologies in situ using spatial frequency domain imaging," Breast Cancer Res. **15**(4), R61 (2013).
15. I. J. Bigio, S. G. Bown, G. Briggs, C. Kelley, S. Lakhani, D. Pickard, P. M. Ripley, I. G. Rose, and C. Saunders, "Diagnosis of breast cancer using elastic-scattering spectroscopy: preliminary clinical results," J. Biomed. Opt. **5**(2), 221–228 (2000).
16. A. M. Zysk, K. Chen, E. Gabrielson, L. Tafra, E. A. May Gonzalez, J. K. Canner, E. B. Schneider, A. J. Cittadine, P. Scott Carney, S. A. Boppart, K. Tsuchiya, K. Sawyer, and L. K. Jacobs, "Intraoperative Assessment of Final Margins with a Handheld Optical Imaging Probe During Breast-Conserving Surgery May Reduce the Reoperation Rate: Results of a Multicenter Study," Ann. Surg. Oncol. **22**(10), 3356–3362 (2015).
17. F. T. Nguyen, A. M. Zysk, E. J. Chaney, J. G. Kotynek, U. J. Oliphant, F. J. Bellafiore, K. M. Rowland, P. A. Johnson, and S. A. Boppart, "Intraoperative Evaluation of Breast Tumor Margins with Optical Coherence Tomography," Cancer Res. **69**(22), 8790–8796 (2009).
18. S. J. Erickson-Bhatt, R. M. Nolan, N. D. Shemonski, S. G. Adie, J. Putney, D. Darga, D. T. McCormick, A. J. Cittadine, A. M. Zysk, M. Marjanovic, E. J. Chaney, G. L. Monroy, F. A. South, K. A. Cradock, Z. G. Liu, M. Sundaram, P. S. Ray, and S. A. Boppart, "Real-time imaging of the resection bed using a handheld probe to reduce incidence of microscopic positive margins in cancer surgery," Cancer Res. **75**(18), 3706–3712 (2015).
19. J. Balog, L. Sasi-Szabó, J. Kinross, M. R. Lewis, L. J. Muirhead, K. Veselkov, R. Mirnezami, B. Dezső, L. Damjanovich, A. Darzi, J. K. Nicholson, and Z. Takáts, "Intraoperative tissue identification using rapid evaporative ionization mass spectrometry," Sci. Transl. Med. **5**(194), 194ra93 (2013).
20. E. R. St John, R. Al-Khudairi, J. Balog, M. Rossi, L. Gildea, A. Speller, R. Ramakrishnan, S. Shousha, Z. Takats, D. R. Leff, and A. Darzi, "Rapid evaporative ionisation mass spectrometry towards real time intraoperative oncological margin status determination in breast conserving surgery.," in *38th Annual San Antonio Breast Cancer Symposium,* (San Antonio, 2016).
21. J. M. Dixon, L. Renshaw, O. Young, D. Kulkarni, T. Saleem, M. Sarfaty, R. Sreenivasan, C. Kusnick, J. Thomas, and L. J. Williams, "Intra-operative assessment of excised breast tumour margins using ClearEdge imaging device," Eur. J. Surg. Oncol. **42**(12), 1834–1840 (2016).
22. A. L. Vahrmeijer, M. Hutteman, J. R. van der Vorst, C. J. van de Velde, and J. V. Frangioni, "Image-guided cancer surgery using near-infrared fluorescence," Nat. Rev. Clin. Oncol. **10**(9), 507–518 (2013).
23. C. Yu, S. Fan, Y. Sun, and E. Pickwell-Macpherson, "The potential of terahertz imaging for cancer diagnosis: A review of investigations to date," Quant. Imaging Med. Surg. **2**(1), 33–45 (2012).
24. S. Fan, Y. He, B. S. Ung, and E. Pickwell-MacPherson, "The growth of biomedical terahertz research," J. Phys. D Appl. Phys. **47**(37), 374009 (2014).
25. A. J. Fitzgerald, V. P. Wallace, M. Jimenez-Linan, L. Bobrow, R. J. Pye, A. D. Purushotham, and D. D. Arnone, "Terahertz pulsed imaging of human breast tumors," Radiology **239**(2), 533–540 (2006).
26. P. C. Ashworth, E. Pickwell-MacPherson, E. Provenzano, S. E. Pinder, A. D. Purushotham, M. Pepper, and V. P. Wallace, "Terahertz pulsed spectroscopy of freshly excised human breast cancer," Opt. Express **17**(15), 12444–12454 (2009).
27. A. J. Fitzgerald, S. Pinder, A. D. Purushotham, P. O'Kelly, P. C. Ashworth, and V. P. Wallace, "Classification of terahertz-pulsed imaging data from excised breast tissue," J. Biomed. Opt. **17**(1), 016005 (2012).
28. C. C. Park, M. Mitsumori, A. Nixon, A. Recht, J. Connolly, R. Gelman, B. Silver, S. Hetelekidis, A. Abner, J. R. Harris, and S. J. Schnitt, "Outcome at 8 years after breast-conserving surgery and radiation therapy for invasive breast cancer: influence of margin status and systemic therapy on local recurrence," J. Clin. Oncol. **18**(8), 1668–1675 (2000).

Biomedical Optics EXPRESS

29. K. S. Khan and P. F. Chien, "Evaluation of a clinical test. I: assessment of reliability," BJOG **108**(6), 562–567 (2001).
30. A. Shalabi, M. Inoue, J. Watkins, E. De Rinaldis, and A. C. Coolen, "Bayesian clinical classification from high-dimensional data: Signatures versus variability," Stat. Methods Med. Res. DOI: 10.1177/0962280216628901 (2016).
31. M. Ahmed, I. T. Rubio, J. M. Klaase, and M. Douek, "Surgical treatment of nonpalpable primary invasive and in situ breast cancer," Nat. Rev. Clin. Oncol. **12**(11), 645–663 (2015).
32. P. C. Ashworth, P. O'Kelly, A. D. Purushotham, S. E. Pinder, M. Kontos, M. Pepper, and V. P. Wallace, "An intra-operative THz probe for use during the surgical removal of breast tumors," in *Infrared, Millimeter and Terahertz Waves, 2008. IRMMW-THz 2008. 33rd International Conference on*, 2008), 1–3.
33. B. C. Truong, H. D. Tuan, A. J. Fitzgerald, V. P. Wallace, and H. T. Nguyen, "A dielectric model of human breast tissue in terahertz regime," IEEE Trans. Biomed. Eng. **62**(2), 699–707 (2015).
34. P. C. Stomper, D. J. D'Souza, P. A. DiNitto, and M. A. Arredondo, "Analysis of parenchymal density on mammograms in 1353 women 25-79 years old," AJR Am. J. Roentgenol. **167**(5), 1261–1265 (1996).

1. Introduction

Breast cancer is by far the most common cancer among women worldwide [1]. A combination of an increased use of screening mammography, neoadjuvant chemotherapy and neoadjuvant endocrine therapy to downstage the size of the tumor, has significantly increased the number of patients suitable for breast-conserving surgery (BCS). Currently approximately two-thirds of newly diagnosed breast cancer patients in the United Kingdom and the United States undergo BCS as initial treatment [2, 3].

A key problem in BCS is that on average approximately 20% of patients require a re-operation because of close or positive tumor margins on postoperative histopathological analysis [4, 5]. Re-operations potentially have a significant impact on patients and healthcare systems. They can result in an increased rate of surgical complications [6], compromise cosmetic outcome [7], delay adjuvant therapy, and increase anxiety and stress for patients and their families. Re-excision surgery also presents a high cost burden to healthcare systems; a recent study in the United States showed that the costs for a re-excision was $4721 per patient [8].

In an attempt to decrease the re-operation rate, techniques to intraoperatively assess tumor resection margins have been developed. Clinically established techniques include specimen radiography, intraoperative ultrasound, radiofrequency spectroscopy, frozen section analysis and touch imprint cytology. However, these all have limitations in terms of diagnostic accuracy, logistical or technical demands or cost-effectiveness [9]. Emerging techniques include Raman spectroscopy [10], diffuse reflectance spectroscopy [11–15], optical coherence tomography [16–18], mass spectroscopy [19, 20], bio-impedance spectroscopy [21], and (targeted) fluorescence imaging [22]. These techniques each have unique limitations, and their potential value for improving quality of care and reducing healthcare costs is yet unknown.

Terahertz pulsed imaging (TPI) employs terahertz (THz) radiation (0.1 – 4 THz) for imaging biological tissue. Due to the millimetric penetration depth and sensitivity of THz radiation to changes in water content and tissue composition, and the submillimeter imaging resolution of TPI, this technique holds promise for imaging cancer [23]. Work performed to date has shown the ability of TPI to discriminate malignant from benign tissue in skin, colon, oral, gastric, brain and breast cancer [24]. In 2006, Fitzgerald *et al.* were the first to demonstrate the potential of TPI for identifying breast cancer during BCS [25]. They measured 22 freshly excised breast tissue samples, and demonstrated a good correlation between tumor size and shape assessed by TPI compared with histopathology. To better understand the origin of the observed contrast on TPI, Ashworth *et al.* used THz spectroscopy and showed that the absorption coefficient and refractive index of tumor were different to that of normal breast tissue in the THz region of the spectrum [26]. Following from their initial work, Fitzgerald *et al.* imaged 51 breast samples and assessed the diagnostic accuracy of TPI by using a range of THz image parameters and classification techniques [27]. They demonstrated an accuracy, sensitivity and specificity of 92%, 90% and 92%, respectively.

Biomedical Optics EXPRESS

However, the TPI device used in their study is not suitable for intraoperative assessment of intact breast specimens due to the requirement for physical tissue disruption to obtain samples that fit the 20 x 20 mm sample holder. Importantly, the tissue samples included in their data set had a 'homogeneous' tissue composition, i.e. contained more than 50% of a single tissue type. This is not an accurate representation of the tissue composition found at the resection border of patients with close or positive margins, as involved margins are often identified microscopically as a small number of tumor cells immersed in a 'background' of fibrous and/or adipose tissue [28]. Thus, the diagnostic accuracy of TPI for detecting tumor close or at the margin remains underdetermined.

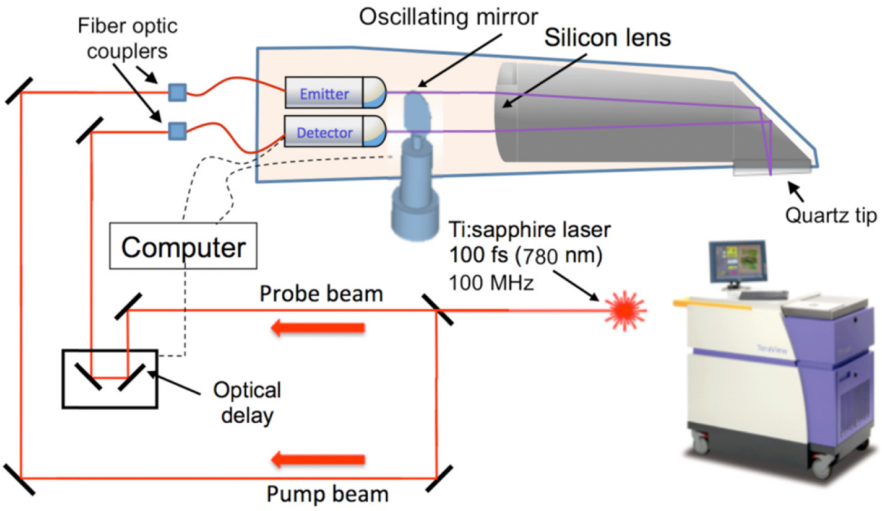

Fig. 1. Schematic illustration of TPI handheld probe system. The emitted laser pulses are split into a "pump beam" and a "probe beam". The pump beam is guided through the optical fibers in the umbilical cord, and subsequently incident on the photoconductive emitter to produce THz pulses. The probe beam is guided onto the photoconductive detector to detect the THz pulses reflected from the tissue sample. By altering the path length of the probe beam, the time of arrival at the detector in respect to the incident THz pulse can be changed, thus sampling the THz pulse in the time domain.

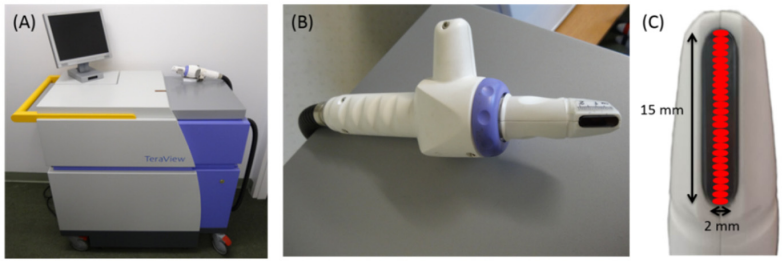

Fig. 2. TPI handheld probe system. (A) Main unit with computer monitor, handheld imaging probe and black umbilical cord (visible on the right). (B) Close up of the handheld imaging probe. (C) Close up of the head of the imaging probe showing the black quartz window. The probe scans an area of 15 x 2 mm, and acquires data from 26 pixels (red).

To facilitate the use of TPI to scan tumor resection margins intraoperatively, Teraview Ltd. (Cambridge, UK) has developed a *handheld* probe system. A single center study was performed to evaluate the ability of the TPI handheld probe to discriminate benign from malignant breast tissue in an *ex vivo* setting. The aims of the study were to obtain a data set that closely resembles the mixture of benign and tumor tissue commonly found at the resection border of patients with involved margins, and to evaluate the diagnostic

Biomedical Optics EXPRESS

performance of the TPI handheld probe in terms of accuracy, sensitivity, specificity and predictive values using two data analysis and classification methods.

2. Methods

2.1 TPI handheld probe system

The TPI handheld probe produces and detects THz pulses by guiding laser pulses from a femtosecond fiber laser (Menlo Systems GmbH, Martinsreid, Germany) down optical fibers to a photoconductive emitter and detector (Fig. 1**)**. The 0.1 – 1.8 THz pulses are then guided by an oscillating mirror via a monolithic silicon section onto a quartz window present at the tip of the probe, scanning 26 pixels in an area of 15 x 2 mm at a frequency of 4 Hz (Fig. 2). During scanning each pixel acquires THz pulses over time to form a TPI image (Fig. 3).

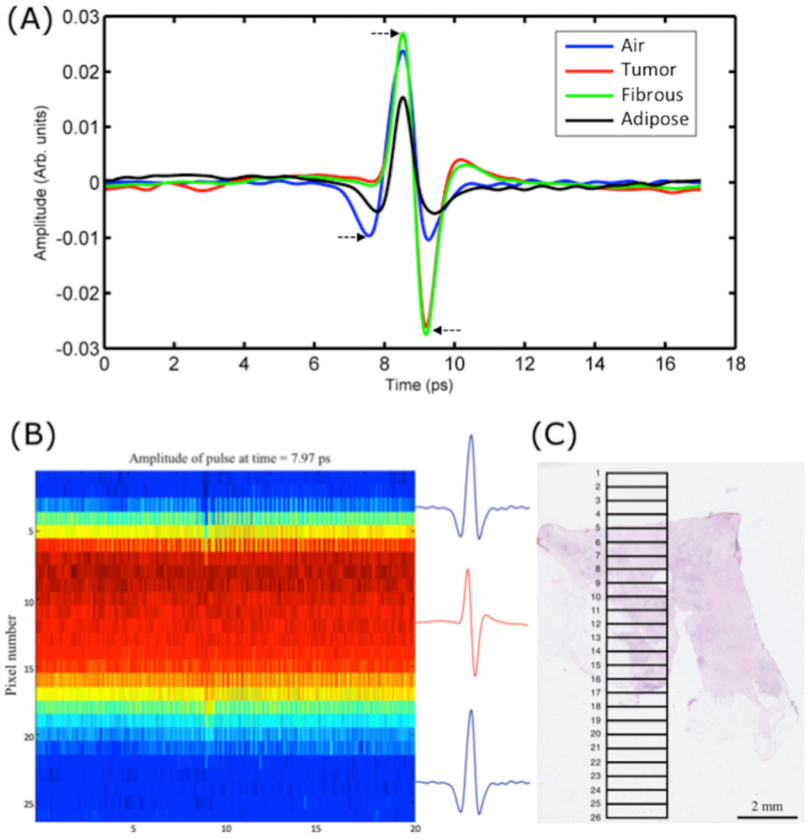

Fig. 3. Correlating TPI with histopathology. (A) Typical impulse function from breast tissue containing a high percentage of tumor, fibrous, and adipose cells, and air, respectively. Clear differences are seen between the impulse functions from air and from tissue, and between adipose and tumor/fibrous tissue, especially at time points t = 7.97 ps, t = 8.93 ps, and t = 9.67 ps (black arrows). (B) TPI image from sample based on the amplitude of the impulse function at t = 7.97ps. A clear contrast can be seen at the air-tissue interface at pixel 5 and pixel 17. Note an 'edge effect' at these interfaces, causing a distortion in the impulse functions of these pixels. (C) Digital histopathology slide of the same tissue sample. By using the photograph of the sample in combination with the air-tissue interface visible in the TPI image, the TPI 15 x 2 mm scan area can be accurately mapped onto the histopathology slide (black rectangle). The pixels are displayed as intermittent horizontal lines at 0.6 mm distance in the scan window. Pixel 5 – 17 contain invasive ductal/no special type (NST) carcinoma; the percentage of tumor cells in each of these pixel areas ranges between 5 – 10%. The tissue immediately surrounding the tumor cells (background) is composed of fibrous tissue, whilst fatty adipose tissue is seen inferiorly.

Biomedical Optics EXPRESS

2.2 Data acquisition

Between August 2013 and August 2014, following written, informed consent, breast tissue samples from patients who underwent BCS or mastectomy at Guy's Hospital in London were scanned with the TPI probe (REC 12-EE-0493). Within 60 minutes post-excision, BCS or mastectomy specimens were inked and sliced by an Advanced Practitioner in the King's Health Partners Cancer Biobank located adjacent to the operating theatre. Tissue samples were obtained for the study subject to the amount of tissue required for diagnostic purposes.

Prior to scanning the samples, a Tegaderm layer (3M Tegaderm Film, 3M, Bracknell, UK) was applied to the probe's quartz window, and the remainder of the probe was wrapped in a disposable protective sheath to prevent contamination from tissue. To enable consistent and controlled TPI measurements, tissue samples were placed in a standard histology cassette (Unisette, Simport, Beloeil, Canada) that tightly fitted the head of the probe (Fig. 4). All samples were scanned for 20 seconds. Upon completion of each measurement a photograph of the sample in the cassette was taken to facilitate accurate correlation of the TPI data with the final histology slide.

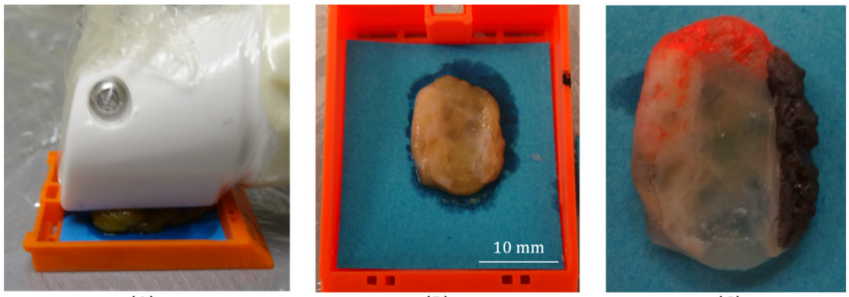

Fig. 4. TPI measurement of tissue sample. (A) TPI handheld probe measurement of tissue sample positioned in histology cassette. Note that the head of the imaging probe tightly fits in the cassette, which facilitates applying a consistent pressure throughout the measurement, while preventing displacement of the probe. (B) Photograph of the tissue sample obtained after the sample was scanned. The imprint of the scan window on the sample is clearly visible. This photograph was used to facilitate accurate correlation of TPI data with histopathology. (C) Photograph of tissue sample after it was inked. Inking was performed to enable spatial orientation of the sample when analysed microscopically by the pathologist.

After the sample was scanned, the Tegaderm layer was removed from the probe and a 60 second air measurement was performed that was used as a reference for data processing. For orientation purposes the top and the right surface of the sample were inked red and black respectively, after which the histology cassette containing the sample was closed, placed in formalin for 24-48 hours, and subsequently processed and paraffin wax embedded. Three to 4 micron sections were then cut and stained with hematoxylin and eosin. The histology slides were digitalized, and subsequently viewed and analyzed using histopathology slide viewer software (NDP.view2, Hamamatsu, UK).

2.3 TPI data processing

Each pixel of the TPI probe acquired raw THz pulses throughout the duration of the measurement. These pulses were deconvolved with the reference ("air without Tegaderm") pulses and a double Gaussian filter was applied to reduce noise. All pulses were aligned in time to compensate for small offsets in the phase of the detected pulses due to changes in the optical path length that occur when optical fibers deform slightly with movement during scanning. The deconvolved pulses – called impulse functions - of each pixel were then averaged over time, resulting in 26 impulse functions, one for each of the 26 pixels to be used for discriminating benign from malignant breast tissue (Fig. 3(B)).

Biomedical Optics EXPRESS

2.4 Correlation of TPI with histopathology

By using the photograph depicting the imprint of the probe's scan window on the sample, and the clear contrast from the air-tissue interface and tissue composition on the TPI image, the 15 x 2 mm TPI scan area was mapped onto the digital histopathology image (Fig. 3(C)). To reduce potential inaccuracies in correlating TPI with histopathology, samples were excluded from further analysis if the number of tissue-containing pixels on TPI and histopathology differed by more than three.

2.5 Histopathological analysis and selection of TPI data

The digital histopathology slide of each sample was analyzed in the viewer software by a Consultant breast histopathologist (S.E.P.), and the percentage of different tissue types, namely tumor, fibrous, and adipose, were recorded in 5% intervals. For a subset of samples an intra-rater variability analysis was performed to assess the ability of the histopathologist to consistently score the tissue samples. For this analysis, a total of 92 pixels from 7 tumor samples and 125 pixels from 7 benign samples were re-evaluated in a blinded method by the same histopathologist 8 weeks after the first analysis. Weighted kappa coefficients were calculated to assess the agreement in subgroup classification between evaluation 1 and 2 (*kappa 2* function of the 'irr' package v0.84, R statistical software v3.2.2). A kappa coefficient (κ) greater than 0.80 was considered excellent agreement [29]. A Wilcoxon signed-rank test was performed to assess whether evaluation 1 was statistically significantly different from evaluation 2. The level of significance was defined as $p < 0.05$.

Table 1. Pixel characteristics analysis data set. A total of 257 pixels were included in the TPI data set: 115 tumor pixels, 116 fibrous pixels and 26 pure adipose pixels. The tumor pixels predominantly consisted of invasive ductal/no special type carcinoma (N = 92) and invasive lobular carcinoma (N = 19). Most of the tumor pixels contained a low to moderate percentage of tumor cells ranging between 1 – 60% (N = 98). Almost all tumor cells had a background of pure fibrous tissue; only 5 had a background containing a mix of fibrous and adipose. Most of the fibrous pixels had a high percentage of fibrous cells ranging between 81 – 100% (N = 91). Only 26 of the 257 pixels consisted of pure adipose tissue.

	Tumor					Fibrous		Adipose
Tissue percentage groups (%)	NST	NST + DCIS	ILC	Number pixels	BG	Number pixels	BG	Number pixels
81 – 100	3	1		4	F	91	A	26[a]
61 – 80	11	2		13	F	2	A	
41 – 60	22		6	28	F	7	A	
21 – 40	33	1	12	46	F: 43 F/A: 3	3	A	
1 – 20	23		1	24	F: 22 F/A: 2	13	A	
Number pixels	92	4	19	115		116		26

NST = invasive ductal/no special type carcinoma; DCIS = ductal carcinoma *in situ*; ILC = invasive lobular carcinoma; BG = background tissue. In our dataset the background consisted of fibrous tissue (F), adipose tissue (A), or a mixture of fibrous and adipose tissue (F/A).

[a]These pixels contained 100% adipose tissue.

Biomedical Optics EXPRESS

2.6 TPI data analysis and classification

Classification of each of the selected impulse functions as malignant or benign was performed using two data analysis and classification methods: (1) heuristic parameters in combination with support vector machine (SVM) classification and (2) Gaussian wavelet deconvolution with Bayesian classification.

The impulse function of each pixel is made of values at 301 time points, and given that information from both the time and frequency domain can be used to classify pixels, it was advantageous to reduce the dimensionality of the data for classification. In method 1 this was done by using parameters that described significant features in the impulse function or spectrum. Since a large number of time points or frequency points can be selected to form a parameter, a Receiver operator Characteristics (ROC) analysis was used to select the optimal characterizing parameters. The area under the ROC curve (AUROC) was used as an estimate of the classification ability of each parameter (illustrated in Fig. 5). AUROC analysis was performed on the data from 3 pathology groups; (i) the entire tumor and fibrous groups (excluding pure adipose), (ii) the tumor and 100% fibrous groups, and (iii) the tumor and 100% adipose groups. From this analysis the top 11 parameters were selected to be used for classification of the data in the SVM (Table 2). To avoid effects of overfitting, the parameters chosen were tested to ensure they were not correlated, eliminating any parameters with an absolute correlation coefficient of 0.7 or more. The SVM function used for classification was from the Matlab native functions *svmtrain.m* and *svmclassify.m* using a radial basis function as the kernel to form the decision boundaries (MATLAB 2013A, The Mathworks Inc., Natick, MA, 2013). A grid search method was applied to optimize the sigma and box constraint terms as 0.3 and 1.1, respectively.

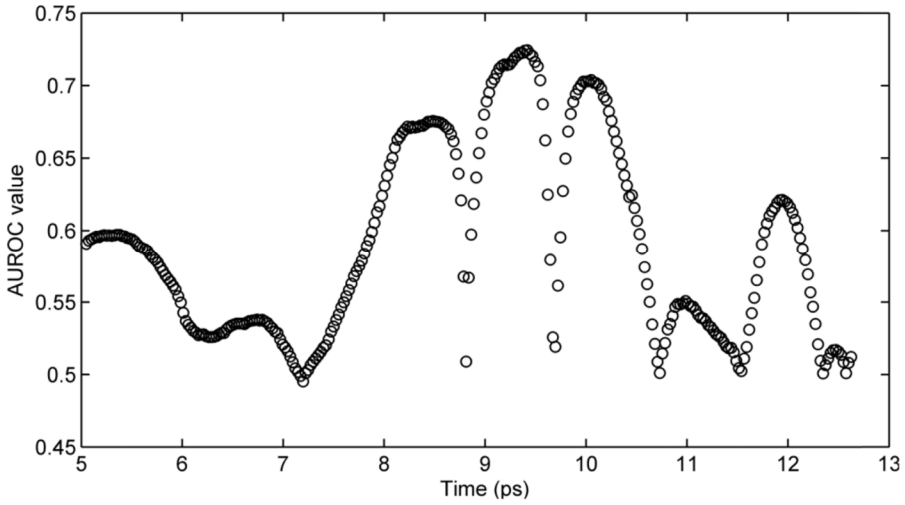

Fig. 5. AUROC analysis to evaluate the discriminative power of the amplitude parameter for time indices 5.0 – 12.6 ps. The highest AUROC values of 0.72 and 0.70 were found at t = 9.42 ps and t = 10.05 ps respectively, and these two parameters were therefore selected for tissue classification with SVM.

Tissue classification was also performed using Gaussian wavelet deconvolution in combination with a Bayesian classifier. In contrast to heuristic parameters, Gaussian wavelet deconvolution can be applied to the full impulse function. This method was considered a suitable approach because of the similarities between the signal features of a Gaussian function and its derivatives, and the TPI impulse functions from breast tissue. Gaussian derivatives of order 0 (normal Gaussian function), 1, 2, 3 and 4 were applied to the impulse function of each pixel. Higher order Gaussian derivatives were not used to avoid potential

Biomedical Optics EXPRESS

overfitting. The Gaussian deconvolved data were then fed into a Bayesian classification algorithm [30], and classified as tumor, fibrous or adipose, respectively. Pixels classified as adipose and fibrous were then grouped together as 'benign' in order to calculate the diagnostic performance of TPI. Similar to SVM, pixels were marked as tumor when containing any amount of cancer cells.

The SVM and Bayesian classifier were trained individually using the leave-one-out method (LOO); leaving out the pixels of a single sample to be classified, and training each classifier on the other samples. The trained classifiers were then applied to the pixels of the sample that was left out. This process was repeated for all the samples, leaving each of them out in turn, and the results compiled to give accuracy, sensitivity, specificity, positive predictive value (PPV), and negative predictive value (NPV) for distinguishing malignant from benign tissue.

3. Results

3.1 Tissue sample characteristics and histopathology intra-rater reliability

In total, 126 samples from 106 patients were scanned; 46 samples from 32 patients met the strict criteria established to ensure accurate correlation of TPI with histology, i.e. a photograph was available of the sample in the histology cassette, and the number of tissue containing pixels on TPI and histopathology differed by 3 or less. These samples were included for analysis. Of these, 20 samples contained tumor; 16 invasive ductal/no special type (NST) carcinoma, 2 NST admixed with DCIS, and 2 invasive lobular carcinoma (ILC). Twenty-two samples contained pure fibrous tissue or a mixture of fibrous and adipose tissue, and 4 samples contained pure adipose tissue. The total number of pixels for analysis was 257; the breakdown in terms of tissue composition is given in Table 1.

The intra-rater reliability analysis showed excellent agreement in cell density subgroup classification between histopathological evaluation 1 and evaluation 2 ($\kappa = 0.89$) ($p = NS$). This confirmed that the established subgroups reliably reflected the tissue composition of the samples, and thus could be used to evaluate the performance of the TPI handheld probe system for different tissue groups.

3.2 Heuristic parameters and SVM classification

A total of 11 parameters were selected based on the AUROC analysis: 10 time domain parameters and 1 frequency parameter (Table 2) (Fig. 6). Most of the time domain parameters capture the area around the minimum amplitude of the pulse, and the return to baseline after the minimum. P1 – P7 were selected based on their overall ability of discriminating tumor from fibrous tissue with adipose, while P8 – P11 were specifically selected to enhance the TPI probe's ability to discriminate tumor from pure fibrous tissue. All 11 parameters showed strong discriminative power to distinguish tumor from pure adipose tissue (mean AUROC = 0.97, range 0.84 – 1.0).

Biomedical Optics EXPRESS

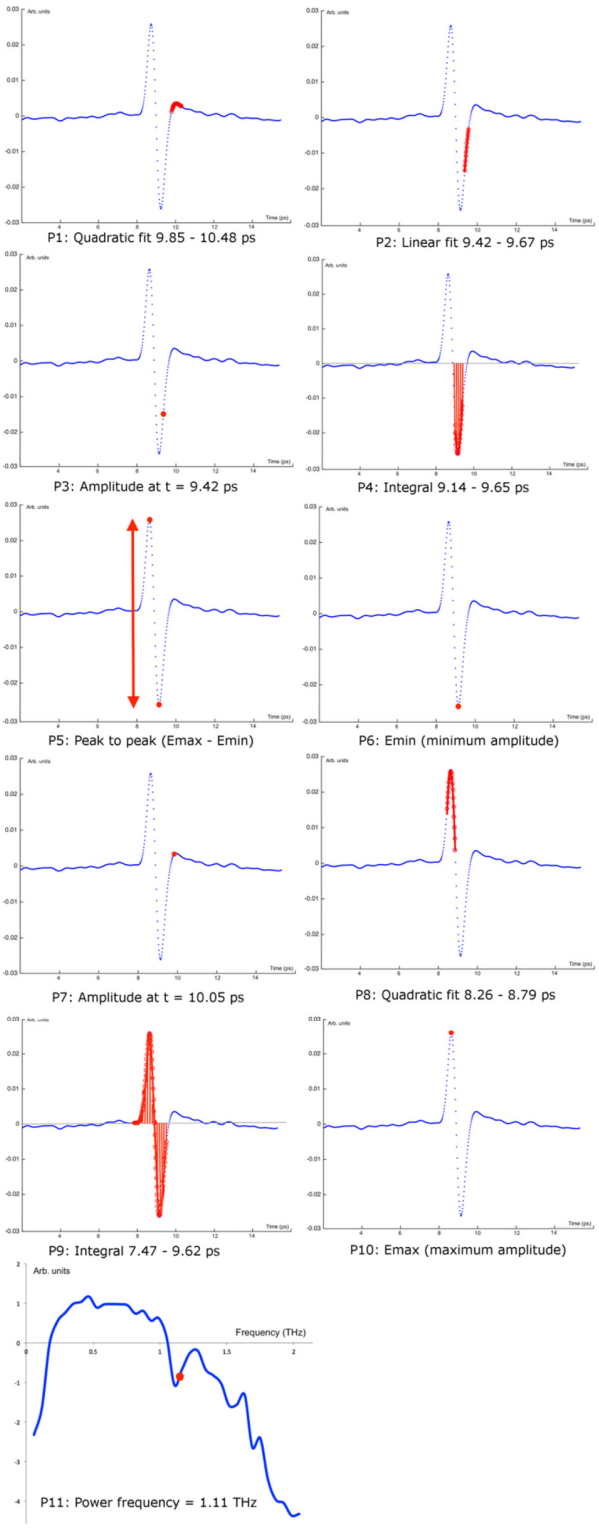

Fig. 6. Visualization of the selected parameters used in SVM classification. Each parameter is displayed in red.

Biomedical Optics EXPRESS

Table 2. Overview of selected time domain and frequency domain parameters and their AUROC values.

Parameter	Definition	AUROC value (cell density group)[a]
P1	*Quadratic fit 9.85 – 10.48 ps*	*0.76 (All T and F)*
P2	*Linear fit 9.42 – 9.67 ps*	*0.73 (All T and F)*
P3	*Amplitude at t = 9.42 ps*	*0.72 (All T and F)*
P4	*Integral 9.14 – 9.65 ps*	*0.72 (All T and F)*
P5	*Peak to peak (Emax minus Emin)*	*0.71 (All T and F)*
P6	*Emin (minimum amplitude)*	*0.70 (All T and F)*
P7	*Amplitude at t = 10.05 ps*	*0.70 (All T and F)*
P8	*Quadratic fit 8.26 – 8.79 ps*	*0.74 (1 – 20% T, 100% F)*
P9	*Integral 7.47 – 9.62 ps*	*0.83 (41 – 60% T, 100% F)*
P10	*Emax (maximum amplitude)*	*0.73 (81 – 100% T, 100% F)*
P11	*Power in spectrum at frequency = 1.11 THz*	*0.82 (61 – 80% T, 100% F)*

[a]T = tumor, F = pure fibrous tissue or a mixture of fibrous and adipose tissue, 100% F = pure fibrous tissue only

The SVM classification results of the individual parameters, and the combination of parameters that performed best in terms of accuracy, may be found in Table 3. Overall, the combination of P1 and P6 provided the best performance with an accuracy, sensitivity, specificity, PPV and NPV of 75%, 86%, 66%, 67% and 85%, respectively. These values were obtained as a result of 16 of the 115 tumor pixels being misclassified as benign; 48 of the 142 benign pixels were misclassified as tumor. All misclassified tumor pixels had a tumor content ≤60%. Of the 48 misclassified benign pixels, 46 were fibrous pixels containing 81 – 100% fibrous cells; only 2 of the 1 – 80% fibrous pixels were misclassified as tumor, and all 26 pure adipose pixels were correctly identified as benign. The two-dimensional parametric plot of P1 and P6 showed very little differences between tumor and high percentage fibrous tissue (Fig. 7(A)); this provides an explanation for why most of the SVM classification errors occurred in these two tissue groups (Fig. 7(B)). Pixels with a high adipose content (1 – 80% fibrous pixels and pure adipose pixels) were generally clearly different from pixels containing a high percentage of fibrous tissue (81 – 100%) and cancer (Fig. 7(A)). The accuracy, sensitivity, specificity, PPV and NPV for discriminating 1 – 80% fibrous and pure adipose tissue from tumor (i.e. excluding the predominantly fibrous group with 81 – 100% purity) was 87%, 86%, 96%, 98%, 75%, respectively.

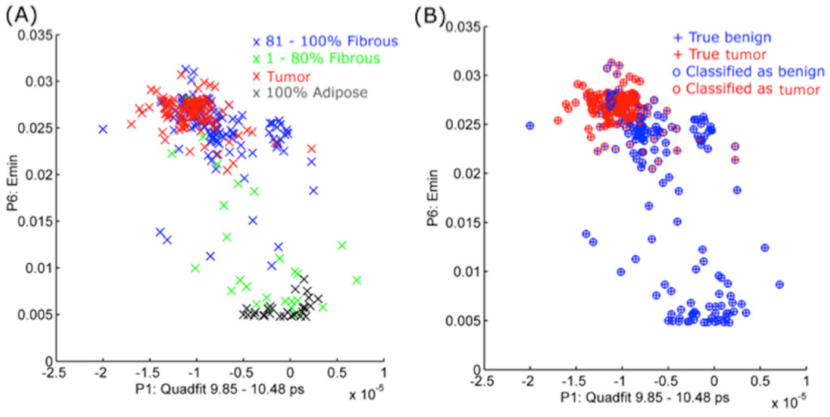

Fig. 7. Two-dimensional parametric plot (A) and SVM classification results (B) for the combination of parameters P1 and P6 that performed best in terms of accuracy.

Biomedical Optics EXPRESS

3.3 Gaussian wavelet deconvolution and Bayesian classification

The accuracy, sensitivity, specificity, PPV and NPV of Gaussian wavelet deconvolution and Bayesian classification was 69%, 87%, 54%, 60%, 84%, respectively (Table 3). Of the 115 tumor pixels, 15 were misclassified as benign. All misclassified pixels contained ≤60% tumor cells. Sixty-six of the 142 benign pixels were wrongly classified as tumor; 64 of these were 81 – 100% fibrous pixels, only two 1 – 80% fibrous pixels were misclassified. All pure adipose pixels were correctly classified. The accuracy, sensitivity, specificity, PPV and NPV of the handheld probe for discriminating 1 – 80% fibrous and pure adipose from tumor was 88%, 87%, 96%, 98% and 77%, respectively.

Table 3. Performance of heuristic parameters with SVM classification, and wavelet deconvolution with Bayesian classification. SVM classification results are shown for individual parameters and parameter combinations that performed best in terms of accuracy. The best individual parameter and parameter combination is underlined.

Parameters	Accuracy (%)	Sensitivity (%)	Specificity (%)	PPV[a] (%)	NPV[b] (%)
P1	*73*	*87*	*62*	*65*	*85*
P2	*72*	*81*	*64*	*65*	*81*
P3	*70*	*77*	*65*	*64*	*78*
P4	*72*	*77*	*69*	*67*	*78*
P5	*72*	*92*	*56*	*63*	*90*
P6	*69*	*86*	*56*	*61*	*83*
P7	*69*	*87*	*54*	*61*	*84*
P8	*68*	*90*	*49*	*59*	*86*
P9	*56*	*69*	*46*	*51*	*64*
P10	*68*	*93*	*48*	*59*	*89*
P11	*56*	*56*	*57*	*51*	*61*
P1 and P6	*75*	*86*	*66*	*67*	*85*
P1, P6 and P11	*71*	*72*	*70*	*66*	*76*
P1, P6, P9 and P11	*67*	*56*	*75*	*65*	*68*
Gaussian wavelets	*69*	*87*	*54*	*60*	*84*

[a]PPV = Positive predictive value

[b]NPV = Negative predictive value

4. Discussion

This study has evaluated the performance of a TPI handheld probe system to discriminate breast cancer from benign breast tissue in an *ex vivo* setting. A total of 257 pixels acquired from scanning 46 breast tissue samples were included for analysis. The tumor samples predominantly contained low-to-moderate tumor cell percentages, resembling the tissue composition found at the resection border of breast specimens from patients with positive margins after BCS. Two data analysis and classification methods were assessed: (1) heuristic parameters in combination with SVM classification and (2) Gaussian wavelet deconvolution with Bayesian classification. On the full data set the former provided the best performance in terms of accuracy (75%). Both methods had excellent sensitivity (86% and 87%, respectively) and thus show promise for identifying tumor cells close to or at the resection margins, allowing immediate further excision of appropriate margins and reducing subsequent second operations/re-excision rates if the TPI handheld probe had been used intraoperatively. Specificity however, was 66% and 54% for SVM and Bayesian respectively; for both methods the lower specificity was due to pixels with 81 – 100% fibrous tissue that were wrongly classified as tumor. The accuracy, sensitivity and specificity increased to 88%, 87%,

Biomedical Optics EXPRESS

and 96% respectively after excluding the 81 – 100% fibrous tissue from the classification results.

The reported pooled sensitivity and specificity of the established techniques to intraoperatively assess tumor margins during BCS are 53% (95% CI 45 – 61%) and 84% (95% CI 77 – 89%) for specimen radiography, 59% (95% CI 36 – 79%) and 81% (95% CI 66 – 91%) for ultrasound imaging, 71% and 68% for radiofrequency spectroscopy, 86% (95% CI 78 – 91%) and 96% (95% CI 92 – 98%) for frozen section analysis, and 91% (95% IC 71 – 97%) and 95% (95% IC 90 – 98%) for imprint cytology, respectively [9]. Thus, based on the results of the present study, the TPI handheld probe appears to perform similarly or better in terms of sensitivity, while the performance in terms of specificity is lower. Compared to specimen radiography and ultrasound, which are also imaging technologies, TPI has the potential advantage that image interpretation is not needed as the device can provide a binary read-out (tumor or no tumor). This may overcome the need for the training required for obtaining ultrasound accreditation [31]. Potential advantages over the histopathological techniques frozen section analysis and imprint cytology are the fact that TPI is non-invasive (i.e. physical tissue disruption is not required), it does not require an on-site cytologist or histopathologist, and allows for assessing a larger tissue surface.

Results published to date on the diagnostic performance of emerging techniques for margin assessment have shown a sensitivity and specificity of 92% (95% CI 86 – 96%) and 97% (95% CI 93 – 98%) for Raman spectroscopy [10], 67 – 85% and 67 – 96% for diffuse reflectance spectroscopy [11–15], 60 – 100% and 69 – 92% for optical coherence tomography [16–18], 93 – 100% and 91.9 – 100% for mass spectroscopy [19, 20], and 87% and 76% for bioimpedance spectroscopy [21], respectively. Although the performance of the handheld probe in this study is somewhat lower than some of the other emerging techniques, TPI uses a different region of the electromagnetic spectrum and thus provides complementary information. It is possible that combinations of technologies could significantly improve the overall accuracy of identifying involved margins.

Several papers have reported on the ability of TPI to discriminate freshly excised benign from malignant breast tissue [25, 27, 32, 33]. Ashworth *et al*. performed a small pilot study using a prototype version of the TPI handheld system [32]; all other studies were conducted with systems not suited for intraoperative imaging of WLE specimens. Similar to the present results, Ashworth *et al.* found that THz impulse functions from fibrous tissue and breast cancer had strong similarities, while impulse functions from adipose tissue had clearly different features. However, none of the TPI studies in breast cancer published to date have used a data set representative of the tissue composition found at the resection border of patients with positive margins, as all tumor samples included for analysis contained >50% tumor cells. Thus, the results in our study are the first that can be used to derive insight in the potential benefits of TPI in enabling more accurate and complete tumor resection in BCS.

The accuracy, sensitivity and specificity of the TPI probe for discriminating tumor from mixed fibrous and adipose tissue, and pure adipose tissue, was 87%, 86%, and 96% for SVM, and 88%, 87% and 96% for Bayesian, respectively. Discrimination of these tissue types is most relevant clinically, as the incidence of breast cancer is higher in older women, who are likely to have fatty or mixed fibrous and fatty breasts compared to younger women who may have more dense breasts primarily composed of fibrous tissue [34].

While the results of this feasibility study are promising, two limitations were noted. Firstly, the 0.6 mm pixel distance used for correlating TPI and histopathology was based on a linear movement of the THz pulse beam across the 15 x 2 mm scan area. However, in practice the THz beam moves faster in the center of the scan window and slows down upon reaching the top and bottom boundary, resulting in a larger distance between pixels located in the center compared to the edges. This introduces a degree of inaccuracy, which was not accounted for in this study. Secondly, the current data set does not contain THz pulses from cases of pure DCIS. These samples could not be assessed, as DCIS is generally non-palpable

Biomedical Optics EXPRESS

and particularly problematic to sample in the fresh state without impairment of gold-standard histological assessment. However, since DCIS is often the cause of the clinical recommendation for re-operations in BCS, it is of key importance to assess the sensitivity of the TPI handheld probe for detecting DCIS. Based on the results of this feasibility study, a study will be performed in which TPI data will be acquired on tissue specimens with DCIS, to determine the ability of TPI to accurately detect DCIS.

In conclusion, the results of this study show that the TPI handheld probe can discriminate invasive breast cancer from benign breast tissue with a high sensitivity and an encouraging degree of accuracy. The main challenge for TPI is accurate discrimination of cancer from tissue containing a high percentage of fibrous stroma due to the similarities in the THz pulse between these two types of tissue. Larger studies are warranted to assess the performance of this technique on different tumor types including DCIS, and its impact on re-operation rate.

Compliance with ethical standards

Ethical approval

All procedures performed in studies involving human participants were in accordance with the ethical standards of the institutional and/or national research committee and with the 1964 Helsinki declaration and its later amendments or comparable ethical standards.

Informed consent

Informed consent was obtained from all individual participants included in the study.

Funding

Guy's and St Thomas' Charity; Academy of Medical Sciences; Cancer Council Western Australia, Youngberg Women's Cancer Research Fellowship (VPW); Australian Government through the Australian Research Council (Discovery Project, DP150100635) and the National Health and Medical Research Council (Development Grant APP1074894).

Acknowledgments

The authors gratefully acknowledge the excellent support from the King's Health Partners Cancer Biobank, Breast Cancer NOW and the breast care team at Guy's Hospital for their help with patient recruitment. In particular we thank Patrycja Gazinska for digitally scanning the histopathology slides.

Disclosures

Michael Pepper and Alessia Portieri are scientific employees of Teraview Ltd; the other authors have no conflicts of interest to disclose.